Wind resource assessment with a mesoscale non-hydrostatic model

Vincent Guénard

Wind resource assessment with a mesoscale non-hydrostatic model

Vincent Guénard, Center for Energy and Processes, ARMINES, Ecole Nationale Supérieure des Mines de Paris, Sophia-Antipolis, France.
vincent.guenard@ensmp.fr

Summary

A new methodology based on high-resolution atmospheric simulations and on the use of the k-means is developed for assessing the wind resource and its uncertainty. The work focuses on an existing wind farm in southern France in the framework of the French EVIDENCE project.

The paper presents the benefits of the use of the k-means approach as a weather situation classification for identifying real and representative meteorological events to simulate by the non-hydrostatic Regional Atmospheric Modelling System (RAMS) model at 200 m horizontal resolution.

The method is validated through comparisons with on-site meteorological mast measurements. The wind speed and turbulence fields are discussed. It is shown that the k-means give both warm (cold) season events for the lower (upper) bound of the wind resource The results show that the turbulent kinetic energy is thermally driven over the targeted area justifying the solving of the full Navier-Stockes equations.

Keywords: wind resource assessment, mesoscale modelling

1 Introduction

Wind resource assessment is a key step for developing wind power energy. From a scientific point of view, it consists in predicting at very high spatial resolutions the wind field of the area of interest for a long period (more than 10 years) corresponding to the life time of the installed wind farm.

This exercice is not an easy task due to the predictability of the non-linear atmospheric processes described by the Navier-Stockes equations (**NS**) that consist of the conservative laws for the mass, momentum, humidity and energy. Solving the full set of **NS** requires such a computational effort that many simplified methods and tools have been developed over these last decades. The simplest methods even do not consider the physics of the Atmospheric Boundary Layer (ABL) by predicting the wind resource with statistical methods only [1].

Other approaches based on a simplified physical modelling filtering out the non-linear processes resulting in linear models such as WASP or MS-Micro.

Parallel to this developments, many efforts have been carried out to improve the numerical weather prediction models either in solving the NS equations with the transition from the hydrostatic to non-hydrostatic models, or in improving the sub-grid parameterisations or the assimilation data schemes. Nowadays, lots of non-hydrostatic mesoscale models are run routinely to give high-resolution weather forecasts (with spatial resolutions ranging from 20 to 1 km, and with time resolution ranging from 3 h to 15 min) [2].

Furthermore, increasing computation power allows us to use these high-resolution atmospheric models in a wind resource assessment context. However, as they require a huge amount of input data for the assimilation schemes, it is still necessary to apply methods for limiting the computational cost.

A method to reduce the computational time consists in simulating randomly selected meteorological events [3]. A more advanced method consists to perform an automatic algorithm that determines the simulated events. For example, clustering methods have been used in wind resource assessment to classify the mean sea level pressure to find representative episodes to statistical downscaling [4]. Principal component analyses have also been used to identify the wind patterns contributing the most to the wind variability [5]. However, the orthogonality of the principal components (both in time and space) have no physical interpretation and can lead to errors when looking for phenomena related to each wind typical pattern [6].The k-means analysis does not present this drawback and has been successfully applied in climatological studies for finding weather regimes by classifying the meteorological events by an iterative algorithm [7]. This method has been

applied to find the episodes to be simulated with the high-resolution MESONH model to determine the wind resource in a very complex terrain in the French Alps [8].

The objective of this study is to extend those works by adding a methodology to assess the uncertainty of the wind resource. The k-means approach is used to determine the events to be simulated with the RAMS non-hydrostatic model at a 200 m spatial resolution. The French EVIDENCE project gives a good framework to reach this goal by gathering the experiences of Natural Power Consultants and Eoleres in wind resource assessment and wind farm exploitations. The study presents the wind resource assessment of the Roussas wind farm in the Rhône valley in Southern France. The wind farm is exploited since 2006 by Eoleres. The site has been instrumented with two high temporal resolution meteorological masts from 2002 to 2004.

The numerical experience consists of four steps. The present paper describes the first of the four step consisting in predicting the wind resource as if no on-site data are available. The on-site measurements are used for the validation of the method only. The second step, to be presented in a future communication, will consist in considering the on-site high temporal resolution data to calibrate the predictions to be compared with the wind measurements carried out in 2006. The third step will consist in performing a wind power resource prediction to be compared with the real power produced in 2006. The fourth step will consist in performing a prediction of the wind power of the wind farm for the next 15 years.

The paper is organised as follows. Section 2 is the description of the Roussas wind farm. The k-means method, the non-hydrostatic atmospheric model and the methodology to derive the uncertainty in the wind resource assessment are described in section 3. The results are shown and discussed in section 4. Concluding remarks and outlooks are given in section 5.

2 Case study

The case study presented here is a wind farm exploited since 2006 in the Rhône valley in southern France. The climatology of the targeted area is governed by two prevailing winds channelled by the valley:

- the northerly wind called the Mistral [9], a cold dry wind affecting the climatology of the north-western Mediterranean either in cold and warm seasons [10] [11]
- the southern wind called the Midi, a warm and moist wind less frequent than the Mistral

The distributions of the Mistral (Fig. 1) and the Midi (Fig. 2) at Montélimar (see Fig. 4 for the location of the meteorological station) show how the Mistral is the dominant of the targeted area. For instance wind speeds greater than 5 m s^{-1} are 10 times more frequent in Mistral situations than in Midi situations.

The Roussas wind farm, operated by Eoleres, is located on a hill crest surrounding the Rhône valley. Its total capacity is 21 MW (12 Vestas V66/1750 wind turbines).

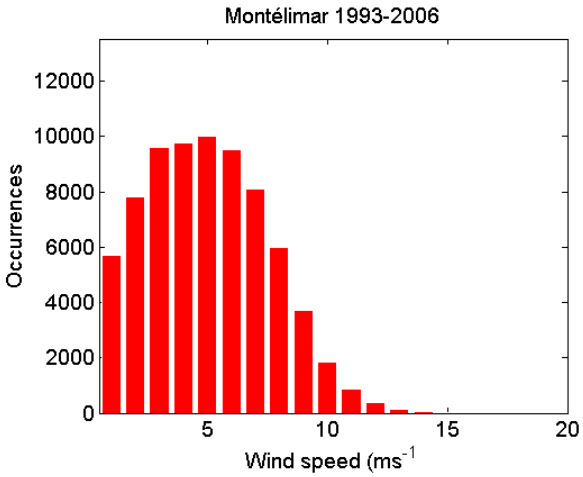

Figure 1: Distribution of the Mistral wind speed measured at Montélimar from 1993 to 2006.

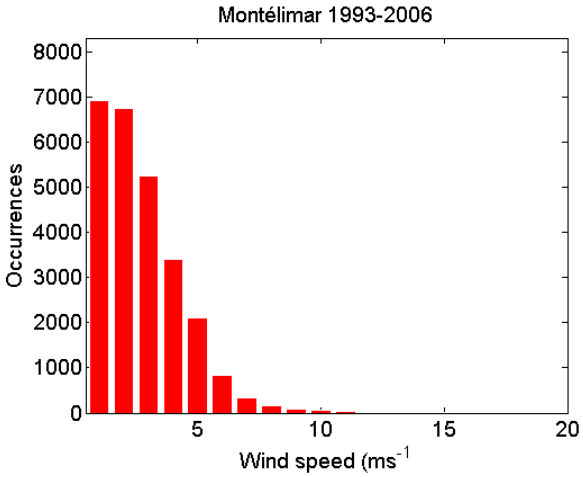

Figure 2: Distribution of the Midi wind speed measured at Montélimar from 1993 to 2006.

3 Methodology

The methodology of this study is based on the use of the RAMS non-hydrostatic atmospheric model to simulate the meteorological fields accurately over the targeted on specific events. The RAMS model is described the first subsection. Those events are determined by the k-means method described in the

second subsection. The wind resource is then derived from a linear combination of the simulated results (subsection 3). The methodology includes also the uncertainty assessment on the wind resource (subsection 4).

3.1 RAMS limited-area model

The RAMS (Regional Atmospheric Modelling System) is a limited-area model solving the primitive set of anelastic **NS** equations using the staggered C grid and the terrain-following vertical coordinate system [12].

The simulations use four two-way nested grids with 25, 5, 1 and 0.2 km horizontal resolutions respectively (see Fig. 3 for the model coverage and Fig. 4 for the 0.2 km horizontal resolution grid coverage). The two coarse (fine) grids are hereafter called mesoscale (microscale). The characteristic of the four grids are summarised in Table 1. The vertical grid spacing, consisting of 36 levels, starts at 40 m and is stretched to 1 km at upper levels to the model top at nearly 23 km.

RAMS uses a full set of physics parameterisations and allows to use different schemes for the parameterisations of the Atmospheric Boundary Layer (ABL) such as the turbulence or the radiative schemes. Two turbulence schemes are implemented depending on the size of the grids. For the mesoscale grids, turbulence is bi-dimensional mainly so that the 2.5 prognostic Turbulent Kinetic Energy (**TKE**) scheme is used [13]. For the microscale grids, the turbulence is three-dimensional. Large Eddy simulation (LES) is performed through the use of the 1.5 prognostic **TKE** scheme [14]. The radiative scheme used describes multi-phase clouds with hydrometeors [15]. For mesoscale grids, the cumulus parameterisation is the modified Kuo deep convection scheme [16]. For microscale grids, the convection is solved explicitly.

The topography and the vegetation cover used by the model are provided by the 30 seconds resolution United States Geological Survey data for the mesoscale grids. For the microscale grids, the 100 m orography is provided by the NASA [17] and the vegetation cover is provided by the Corine Land Cover 2000 data base. The sea surface temperature has been provided by monthly climatological series with 80 km horizontal resolution.

In this study, RAMS is driven by the European Centre for the Medium-range Weather Forecast (ECMWF) analyses specifying its initial and boundary conditions every 6 h on a 0.25 °× 0.25 ° latitude-longitude grid (around 25 km resolution).

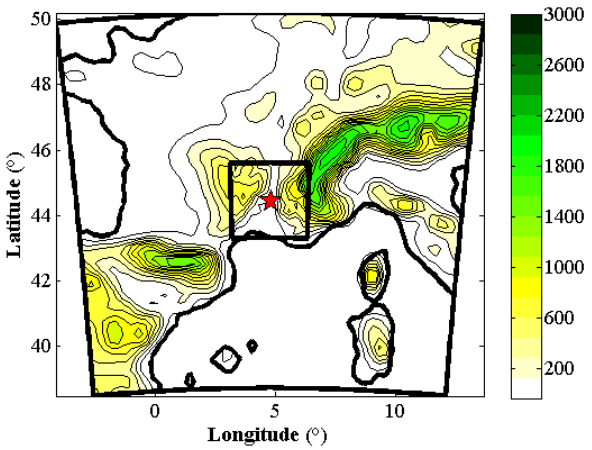

Figure 3: Targeted domains of numerical simulations for the mesoscale grids. The relief is given in meters. The red star gives the location of the Roussas wind farm. The frames gives the coverage of the RAMS nested grids with 25 and 5 km horizontal resolutions.

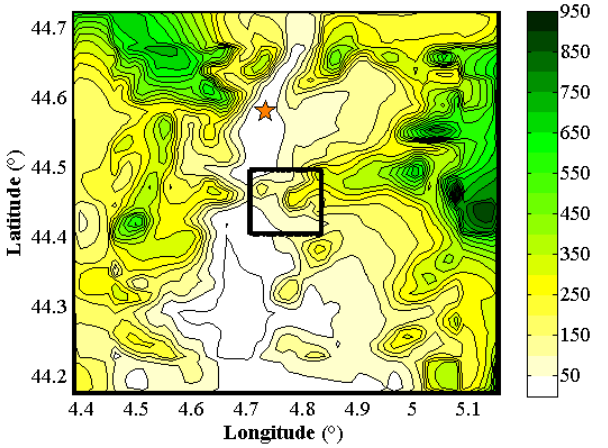

Figure 4: Targeted domains of numerical simulations for the microscale grids. The relief is given in meters. The orange star gives the location of the meteorological station at Montélimar. The frames gives the coverage of the RAMS nested grids with 1 and 0.2 km horizontal resolutions.

	mesoscale		microscale	
grid	1	2	3	4
resolution (km)	25	5	1	0.2
number of points in horizontal	2704	5184	3844	2704
number of points in vertical	36	36	36	36

Table 1: RAMS grid configurations for the prediction of the wind resource of the Roussas wind farm.

3.2 k-means

The k-means approach has been performed successfully in climatology to identify weather

patterns [7]. from synoptic pressure fields. Here, the 500 hPa geopotential fields over Western Europe of the last 15 years ECMWF operational analyses are analysed. Their spatial resolution is 1°. Their time resolution is 6 h that represents more than 21000 analyses.

In the k-means, the number of selected events ***N*** has to be prescribed. Each field has been randomly distributed in the ***N*** bins. An iterative algorithm minimises the distance between the fields of each bin while maximising the variance of the mean fields of the ***N*** bins. The distance chosen is the euclidean distance.

This method is convergent absolutely constituting its major interest [7]. However, this method is sensitive to the initial configuration resulting in convergence to local extrema. As recommended by the community, several initial configurations have been tested as well as several ***N*** values ranging from 8 to 40. The upper limit is determined by the computational time available. The criterion determining ***N*** is the level of variance of the mean fields of the ***N*** bins. 18 events have been found.

The closest meteorological events from the 18 **centroids** of the 500 hPa geopotential fields (in terms of the euclidean distance) with a minimum duration of 24 h to enclose the diurnal cycle have to be simulated by the non-hydrostatic mesoscale model. Actually, the effective simulated events are anticipated from 24 h and extended for 24 h for two major reasons leading to 72 h simulated events. It allows:

- a better simulation of the targeted event (less dependent from the analyses of the global model)
- a computation of the uncertainty of the method as described in subsection 4

3.3 Wind resource assessment

The central 24 h simulated event of each simulation is extracted and weighted by the frequency of occurrence of each event. This frequency is the number of elements of the ***N*** bins divided by the total number of elements. The wind resource is therefore the sum of the weighted wind speed (**WS**) fields.

The interest of using a non-hydrostatic atmospheric model is the assessment of the vertical velocity (**w**) and the **TKE** fields as they are computed directly from the conservative **NS** equations. Furthermore, the fields can be computed from different levels in the ABL having an information on dynamical shear stresses. The resulting **WS**, **w** and **TKE** fields are analysed in Section 4.

3.4 Uncertainty assessment

The uncertainty of the whole method is threefold:

- errors from the non-hydrostatic model to simulate the meteorological fields accurately due to three main causes (hereafter called the physical error **PE**): the low predictability of the atmospheric processes governed by the non-linear NS equations, the approximated physics used to solve sub-grid processes, and errors in the description of the state of the atmosphere at a given time impacting the assimilation schemes. **PE** can be evaluated by comparing the simulated results to real measurements (given by meteorological stations and/or on-site measurements)
- errors from the k-means due to two causes (hereafter called the statistical error **SE**): errors in the representativeness of **N** centroids of the elements of the **N** bins, errors due to a slight differences between the **N** centroids and the **N** real events to simulate. **SE** can be evaluated by simulated the **N** events the farthest from the centroids (hereafter called **extremes**). It results in multiplying by two the computational cost (**2N** 72 h-simulations)
- errors from using the non-hydrostatic model and the k-means together (hereafter called the statistical-physical error **SPE**). One specific meteorological event of the **i** bin is represented by the simulated event of the **i** bin, **SPE** can be evaluated by comparing the simulated results for each run from 0-to-23 and 48-to-72 h with the specific meteorological event

The chosen error measure is the absolute error. The total uncertainty is then **PE + SE + SPE**. Only the evaluations of **PE** obtained by comparisons simulations/observations at the Montélimar meteorological station and **SE** are available for the Roussas case study. These results and discussed in section 4.

4 Results

This section gives the results of the k-means (subsection 1), of the RAMS simulation (subsection 2).

4.1 Meteorological situation-types

Table 2 gives the occurrence frequencies of the 18 events. One can notice that the 18 situations are quite homogeneous with frequencies ranging from 3 to 8 %. Figures 5-to-8 are some examples of the

dimensionless 500 hPa geopotential height field for the four events numbered by 3, 10, 12 and 14.

Event	Occurrence frequency (%)
1	4.87
2	5.69
3	6.58
4	6.14
5	3.84
6	2.96
7	5.04
8	5.43
9	5.59
10	5.97
11	7.42
12	5.90
13	4.40
14	7.68
15	6.23
16	6.95
17	3.96
18	5.20

Table 2: Occurrence frequencies (%) of the 18 events to be simulated by RAMS model. They are used as weights of the RAMS simulations for the wind resource assessment.

The event 3 (Figure 5) is characterised by the Biscay low and the high over the North Sea. This typical meteorological situation occurring in spring or autumn mainly, leads to a easterly flow over southern France.

The event 10 (Fig. 6) is characterised by the low over the Atlantic while the high is located in northern Mediterranean. This meteorological situation occurring in spring or autumn leads to southerly flow in southern France and is typical for triggering the Midi.

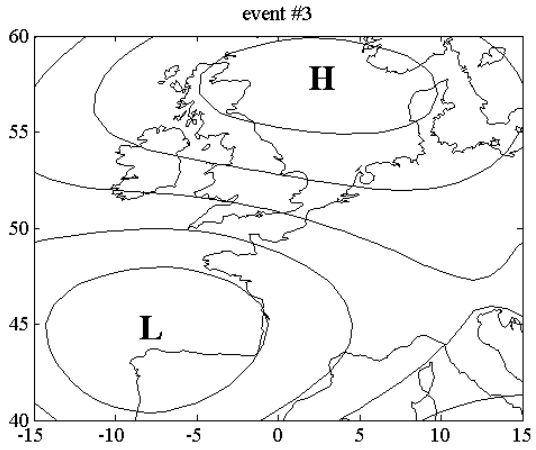

Figure 5: Centroid for the event 3 on the 500 hPa dimensionless geopotential height corresponding to the 17th October 2003 at 06Z. L (H) denotes the low (high) pressure.

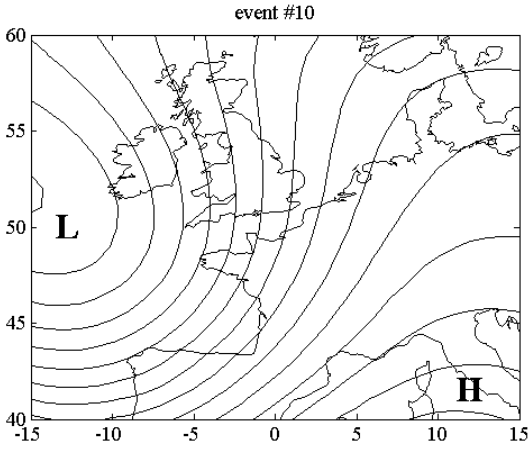

Figure 6: Centroid for the event 10 on the 500 hPa dimensionless geopotential height corresponding to the 101h June 1997 at 12Z. L (H) denotes the low (high) pressure.

The event 12 (Fig. 7) is characterised by the low over Italy while the Azores ridge is located over the Iberian peninsula. This meteorological situation occurring in winter leads to northerly flow in Southern France and is typical for triggering the Mistral [10].

The event 14 (Fig. 8) is characterised by the low over the northern Atlantic while the high is located in southern Mediterranean. This typical meteorological situation occurring in summer leads to calms in southern France.

The k-means has proven to be a very efficient method for identifying typical meteorological situations over western Europe. For each event, the real episode which is the closest (farthest) from the centroid (extreme) determined by the k-means method is simulated by the non-hydrostatic atmospheric model at a 200 m horizontal resolution over the targeted area.

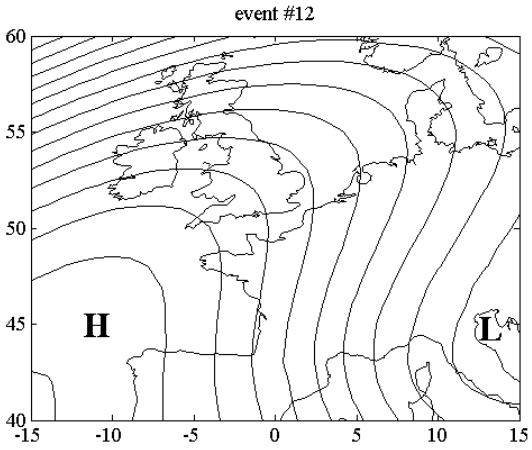

Figure 7: Centroid for the event 12 on the 500 hPa dimensionless geopotential height corresponding to the 26th June 1996 at 18Z. L (H) denotes the low (high) pressure.

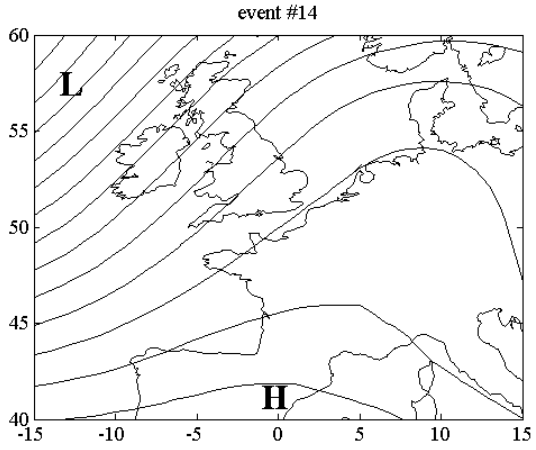

Figure 8: Centroid for the event 14 on the 500 hPa dimensionless geopotential height corresponding to the 10th September 2006 at 12Z. L (H) denotes the low (high) pressure.

4.2 Mesoscale modelling

Four examples of 10 m wind speed fields simulated by RAMS are displayed in Figures 9-to-12. They correspond to the synoptic situations described by the Figures 5-to-8 respectively. They are extracted for the coarsest mesoscale grid at a 25 km horizontal resolution. Each field participates in building the wind resource of the targeted area with a weight of $\mathbf{f_{occ}/24}$ where $\mathbf{f_{occ}}$ is the occurrence frequency of the corresponding event to be divided by the number of hours in a day.

Figure 9 illustrates a severe easterly wind over the Mediterranean with calm situations within the Rhône valley.

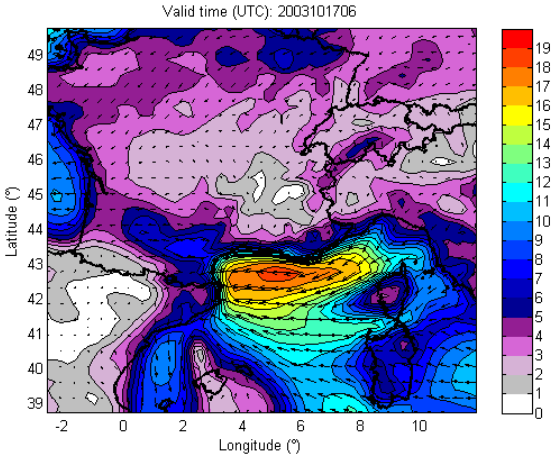

Figure 9: 10 m wind speed field simulated by RAMS at a 25 km horizontal resolution on the 17th October 2003 at 06Z. The wind direction is given by arrows and the wind speed (m s-1) by colours. This fields participates in building the event 3 (Fig. 5).

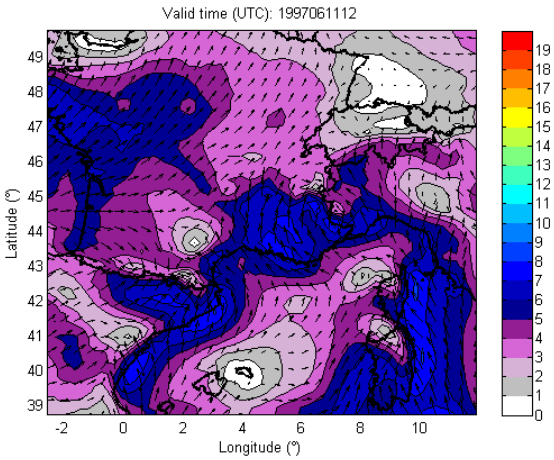

Figure 10: 10 m wind speed field simulated by RAMS at a 25 km horizontal resolution on the 11th June 1997 at 12Z. The wind direction is given by arrows and the wind speed (m s-1) by colours. This field participates in building the event 10 (Fig. 6).

Figure 10 illustrates the Midi channelled by the Rhône valley.

Figure 11 displays a typical Mistral event where the northerly flow is channelled by the Rhône valley and veers south-eastward over the Mediterranean.

Figure 12 illustrates a weak easterly flows leading to calm situations within the Rhône valley.

It must be noted that all the Mistral cases are not provided by the event 12 only; 9 other events involves the Mistral as it can be induced by different pressure configurations [10].

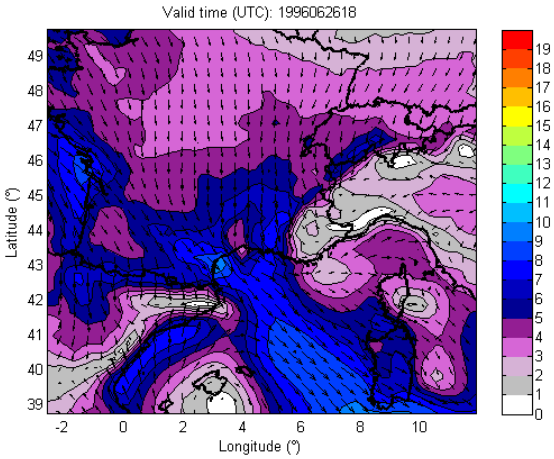

Figure 11: 10 m wind speed field simulated by RAMS at a 25 km horizontal resolution on the 26th June 1996 at 18Z. The wind direction is given by arrows and the wind speed (m s-1) by colours. This field participates in building the event 12 (Fig. 7).

Similar methodologies are applied on the results of the extreme simulations for determining the term **SE** of the uncertainty.

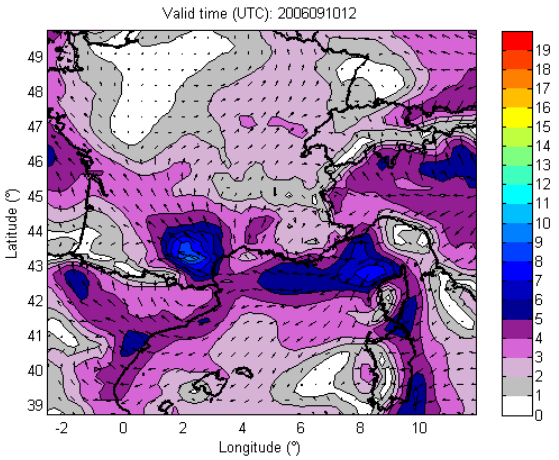

Figure 12: 10 m wind speed field simulated by RAMS at a 25 km horizontal resolution on the 10th September 2006 at 12Z. The wind direction is given by arrows and the wind speed (m s-1) by colours. This field participates in building the event 14 (Fig. 8).

4.3 Validation

The validation phase consists of comparisons between the measured wind speeds and directions at Roussas carried out by EOLERES from 2002 to 2004 and the k-means-rams predictions for the same period. Figure 13 presents the wind roses computed from the on-site measurements and from the predictions for centroids and extremes given by the k-means method.

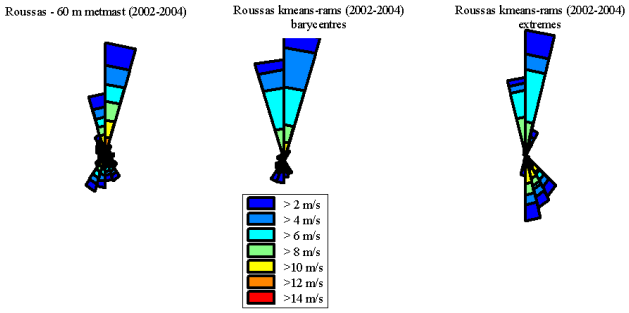

Figure 13: Wind roses computed from (left) the measurements at Roussas between 2002 and 2004, (center) k-means-RAMS centroid predictions (right) k-means-RAMS extreme predictions for the same period.

From the wind rose analysis, it appears clearly that the proportion of dominant wind is well predicted. These results are very encouraging. However, differences can be found in the magnitude of the wind speeds. Furthermore, it can be seen that some information from the centroids are missing especially on the occurrence of the Midi. However, it can be noted that extreme situations give the missing information. The reason for that is that centroid situations have been found during the warm season when the Midi is seldom while extreme situations have been found during the cold season when the Midi is the most frequent. It does not affect the Mistral description since it is present throughout the year [10].

Table 3 gives the monthly temperature measured at Montélimar from 1986 to 2005. It evidences that the cold season (when temperature lowers the annual value) can be defined from November to April. The warm season is then from May to October. The monthly repartition of the simulated events are also reported in Table 3. All the centroid events are in the warm season and more than 90 % of the extremes are in the cold season (The remaining events are in October not far from the cold season). The averaged temperature predicted over the Roussas area 20.9 °C for centroids and 7.1 °C for extremes.

	Montélimar		kmeans-rams	
	T (°C)	WS (m/s)	Barycentres	Extremes
JAN	5.3	3.9	0	5
FEV	6.5	4.1	0	4
MAR	10.1	4.2	0	0
AVR	12.1	4.0	0	1
MAY	17.0	3.6	2	0
JUN	20.5	3.8	4	0
JUL	23.3	4.1	5	0
AUG	23.4	3.6	2	0
SEP	18.8	3.6	2	0
OCT	14.7	3.1	3	2
NOV	8.9	4.0	0	3
DEC	6.0	4.0	0	3
Tmean (°C)	13.9	3.8	20.9	7.1

Table 3: Monthly averaged temperature and wind speed observed from 1986 to 2005 at Montélimar (From Météo-France) and monthly repartition of the events for centroid and extreme simulations. Cold (warm) season are displayed in blue (red).

The origin of the separation between centroid/warm and extreme/cold can be found in the classifying algorithm of the k-means method. Similar configurations within each group from cold and to warm seasons differ by the magnitudes of the pressure gradients. The pressure gradients are generally weaker in the warm than in the cold seasons directly impacting the classification within each group. The effect of finding the centroid is similar as finding smoothed fields explaining that the centroids are found in warm seasons generally. On the opposite side, the extremes are therefore found in cold seasons.

This finding allows to consider again the method to predict the wind resource and its uncertainty. Here, the centroid simulations must be taken as the lower limit of the wind resource as warm seasons are generally characterised by weaker winds (Table 3).

The extreme simulations are thus the upper limit of the wind resource.

4.4 Wind resource

This subsection gives the geophysical resources at Roussas as predicted by combining the k-means with very high resolution RAMS simulations.

Figure 14 gives the **WS** resource at 60 m Above Ground Level (AGL) at Roussas from the centroid simulations. One can notice the wind speed acceleration over the hill crest in the range of 8-9 m s^{-1}. The mean wind speed of the wind farm is predicted to be at around 7 m s^{-1}.

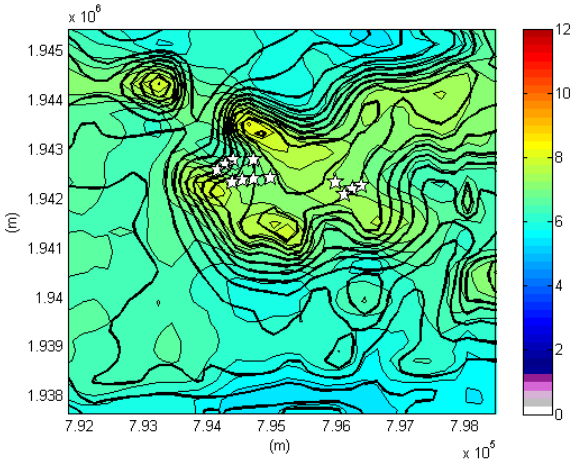

Figure 14: Horizontal wind speed resource at 60 m AGL for the Roussas wind farm computed from the centroid simulations. The colours give the wind speed in m s^{-1}. Thick black lines are the orography contours. White stars give the wind turbine positions.

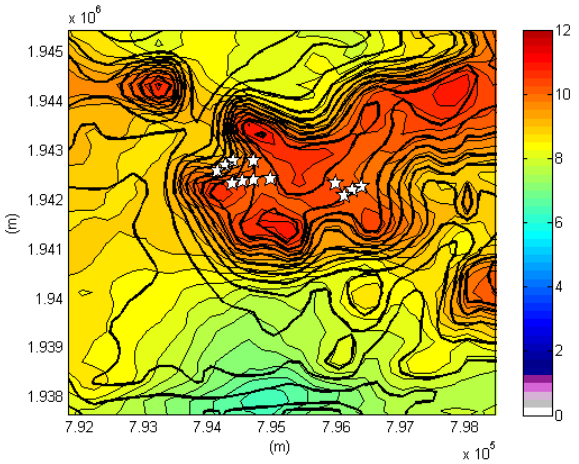

Figure 15: The same as Fig. 14 for the horizontal wind speed (m s^{-1}) of the extreme simulations.

Figure 15 gives the **WS** resource at 60 m AGL at Roussas from the extreme simulations. It is clear that in cold seasons, the wind is stronger. Over the whole finest microscale grid, the mean wind speed is predicted at 6.1 m s^{-1} on warm seasons and at 8.5 m s^{-1} in cold seasons leading to a 30 % difference.

Figure 16 gives the **w** resource at 60 m AGL from the centroid simulations. As the northerly wind prevail, upward winds are predicted over the northern hillside in the 0.3-0.5 m s^{-1} range. Downward velocities of similar magnitudes are predicted in the southern hillside.

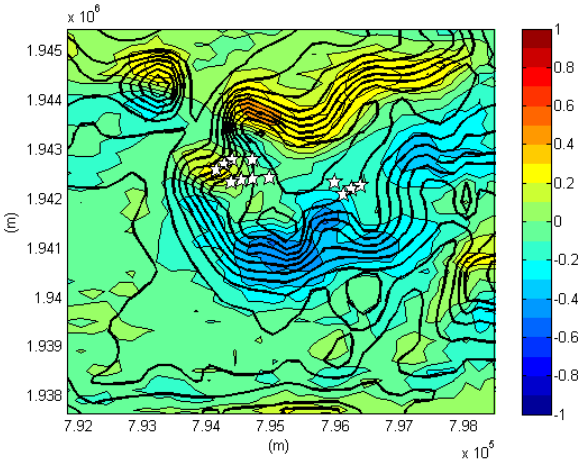

Figure 16: The same as Fig. 14 for the vertical wind speed (m s^{-1}) of the centroid simulations.

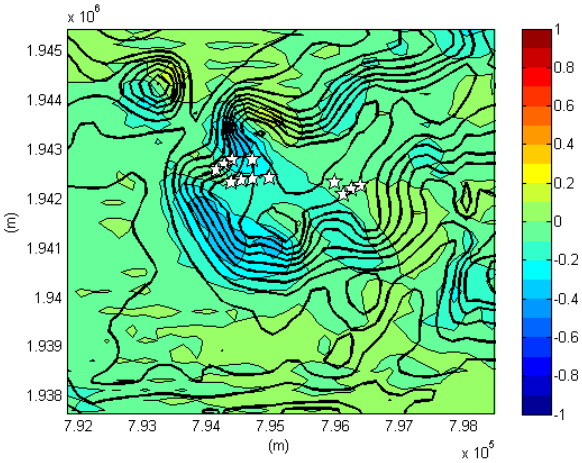

Figure 17: The same as Fig. 14 for the vertical wind speed (m s^{-1}) of the extreme simulations.

Figure 17 gives the **w** resource at 60 m AGL from the extreme simulations. The locations of upward and downward motions is still unchanged in cold seasons. However, one can notice that their respective magnitudes are predicted to decrease in cold seasons leading to a more horizontal flow since the horizontal winds are predicted stronger than in warm seasons.

Figure 18 gives the **TKE** resource at 60 m AGL from the centroid simulations. Turbulence is predicted to be higher between the two hill crests on the north-western hillside as well as in the southern hillside where downward motions are predicted.

Figure 19 gives the **TKE** resource at 60 m AGL from the extreme simulations. The locations of the predicted highest turbulence are similar in cold than in warm seasons. However, one can notice that the mean intensity of **TKE** is predicted to be higher in warm than in cold seasons. Over the whole finest microscale grid, the mean **TKE** is predicted at 1.48 $m^2 s^{-2}$ on warm seasons and at 1.24 $m^2 s^{-2}$ in cold seasons leading to a 17 % difference. As **TKE** is greater in warm and weak windy conditions than in cold and high windy conditions, it is clear that its main origin is rather the buoyancy than the vertical shear effects. Hence, it evidences the benefits to solving at the same time the mass, momentum, humidity and **TKE** conservative laws.

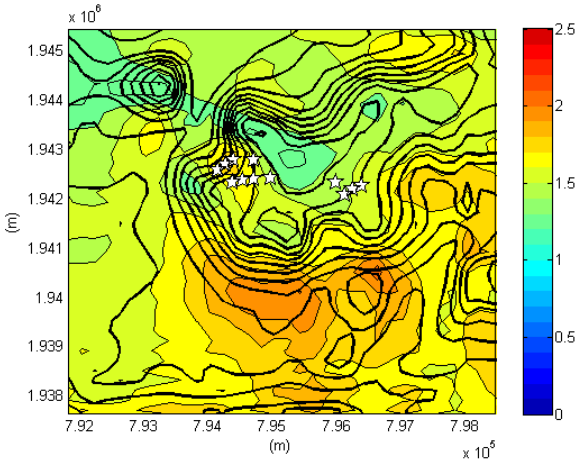

Figure 18: The same as Fig. 14 for the turbulent kinetic energy ($m^2 s^{-2}$) of the centroid simulations.

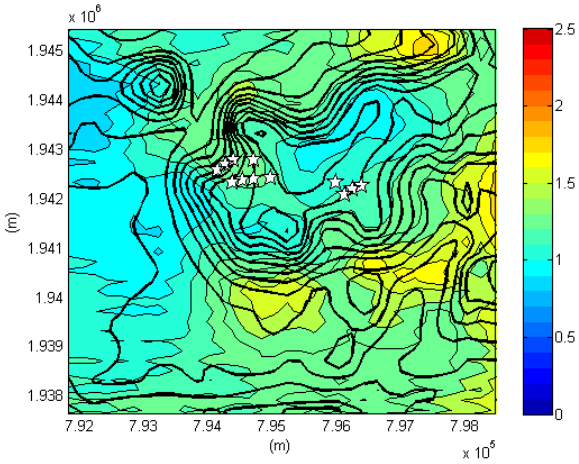

Figure 19: The same as Fig. 14 for the turbulent kinetic energy ($m^2 s^{-2}$) of the extreme simulations.

5 Conclusions

This work is the first step toward a full-validated methodology to predict the wind resource and its uncertainty. It consists in finding representative meteorological events with the k-means classifying method to be simulated with a very high-resolution (200 m) non-hydrostatic numerical model. The work has shown the ability of the k-means to find representative warm episodes as centroids and cold episodes as extremes. This property will be used to predict the wind resource assessment and its uncertainty as well. The combination of k-means-rams highlights the realism for the prediction of the wind roses computed by on-site meteorological masts installed from 2002 to 2004. This work has also shown the ability of the RAMS model to perform very high-resolution simulations thanks to the several implemented parameterisations especially the possibility to switch from two turbulence parameterisations.

The second step of this work will consist in computing a Model Output Statistics (MOS) corrections of the predicted meteorological fields displayed in subsection 4.4 based on the on-site meteorological mast measurements. The third step will consist in performing a wind power resource prediction based of the installed wind turbine power curves to be compared and validated with the real power produced in 2006. The fourth step will consist in performing a prediction of the wind power of the wind farm for the next 15 years.

This methodology will also be applied to predict the wind resource of the Crystal Rig and Windy Standard Scottish wind farms operated by Natural Power.

The present work shows the benefits from using more advanced models for the wind resource assessment for the new installation of complex wind farms presenting more financial risks.

Acknowledgements

This work is the contribution in the task “Physical modelling of the wind resource and its uncertainty” of the EVIDENCE project that is supported by the French Agency for Environment and Energy Management (ADEME). The author would like to thank ECMWF for providing the global model analyses and Météo-France for providing climatological data. The authors are also thankful for all the efforts made by the RAMS community.

References

[1] Rogers, A. L., J. W. Rogers, and J. F. Manwell, 2005: Comparison of the performance of four measure-correlate-predict algorithms. *J. Wind Engin. Ind. Aerodyn.*, **93**, 243-264.

[2] Baklanov, A., B. Fay, and J. Kaminski, 2007: Overview of existing integrated (off-line and on-line) mesoscale systems in Europe. *Cost Action 728,* Deliverable 2.1, 162 pp.

[3] Yu, W., R. Benoit, C. Girard, A. Glazer, D. Lemarquis, J. R. Salmon, and J. P. Pinard, 2006: Wind Energy Simulation Toolkit (WEST): a wind mapping system for use by the wind-energy industry. *Wind Engin.*, **1**, 15-33.

[4] Barquero,C. G., I. Martí, M. Marchante, J. Navarro, and L. Corrochano, 2000: Wind power prediction by cluster analysis in Spain. *Proc. Wind Power for the 21st century*, 25-27 September 2000, Kassel, Germany.

[5] Hardy, D. M., and J. J. Walton, 1978: Principal components analysis of vector wind measurements. *J. Appl. Meteor.*, **17**, 1153-1162.

[6] Kalkstein, L. S., G. Tan, and J. A. Skindlov, 1987: An evaluation of three clustering procedures for use in synoptic climatological classification. *J. Appl. Meteor.*, **26**, 717-730.

[7] Michelangeli, P. A., R. Vautard, and B. Legras, 1995: Weather regimes: recurrence and quasi stationnarity. J. Atmos. Sci., 52, 1237-1256.

[8] Soulan, I., and C. Lac, 2005: Etude du gisement régional éolien sur la zone Alpine. Rhônalpénergie environnement - Météo France, Technical report, 37 pp.

[9] Pettré, P., 1982: On the problem of violent valley winds. J. Atmos. Sci., **39**, 542-554.

[10] Guénard, V., P. Drobinski, J.L. Caccia, B. Campistron and B. Bénech, 2005: An observational study of the mesoscale Mistral dynamics. *Bound-Layer Meteor.*, **115**, 263-288.

[11] Guénard, V., P. Drobinski, J. L. Caccia, G. Tedeschi, and P. Currier, 2006: Dynamics of the MAP IOP 15 severe Mistral event: Observations and high-resolution numerical simulations. *Quart. J. Roy. Meteor. Soc.*, **132**, 757-777.

[12] Pielke, R. A., W. R. Cotton, R. L. Walko, C. J. Tremback, W. A. Lyons, L. D. Grasso, M. E. Nicholls, M. D. Moran, D. A. Wesley, T. J. Lee, and J. H. Copelandand, 1992: A comprehensive meteorological modelling system – RAMS. *Meteor. Atmos. Phys.*, **49**, 69-91.

[13] Mellor, G. L, and T. Yamada, 1982: Development of a turbulence closure model for geophysical fluid problems. *Rev. Geophys. Space Phys.*, **20**, 851-875.

[14] Deardoff, J. W., 1980: Stratocumulus-capped mixed layers derived from a three-dimensional model. *Bound-Layer Meteor.*, **18**, 495-527.

[15] Harrington, J. Y., T. Reisin, W. R. Cotton, S. M. Kreidenweis, 1999: Cloud resolving simulations of Arctic stratus. Part II: Transition-season clouds. *Atmos. Res.,* **55**, 45-75.

[16] Tremback, C. J., 1990: Numerical simulation of a mesoscale convective complex: model development and numerical results. Ph.D. dissertation, Atmos. Sci. Paper No. 465, Department of Atmospheric Science, Colorado State University, Fort Collins, CO 80523, 247 pp.

[17] Rodriguez, E., C. S. Morris, J. E. Belz, E. C. Chapin, J. M. Martin, W. Daffer, S. Hensley, 2005: An assessment of the SRTM topographic products. *Jet Propulsion Laboratory*, JPL D-31639 Technical report, 1435-1470.